CORRELATION BETWEEN MINORITY CARRIER DIFFUSION LENGTH AND MICROSTRUCTURE IN a-Si:H THIN FILMS

G. Conte*, G. Fameli*, G. Nobile*, A. Rubino*, E. Terzini*, F. Villani*, D. Caputo**, G. de Cesare**, F. Irrera**, F. Palma** and M.C. Rossi**
* ENEA - Centro Ricerche Fotovoltaiche, P.O.Box 32, 80055 Portici (Na), Italy
** Università di Roma "La Sapienza", Dipartimento di Ingegneria Elettronica, Via Eudossiana 18, 00184 Roma, Italy

ABSTRACT

Aim of this work is to investigate the opto-electronic properties of amorphous hydrogenated silicon (a-Si:H). The deposition temperature has been used as a driven force to modify the morphology and bonded hydrogen distribution. The influence of the hydrogen microstructure on the carriers $\mu\tau$ product has been examined. The $\mu\tau$ products, for both carriers, have been evaluated from the diffusion length measurement, by using the Steady State Photocarrier Grating (SSPG) technique, and from the photoconductivity in the steady state condition (SSPC). The $\mu\tau$ products have been correlated with the defect density and Fermi level position. The effects of the defect density on the Fermi level position has been examined within the frame of a defect pool model in order to justify the consistence of the results.

INTRODUCTION

During the past few years a lot of efforts have been devoted to study the influence of the hydrogen microstructure on the transport properties of a-Si:H thin films. It is generally accepted that this material does not consist of a homogeneous random network, but rather of the mixture of a well-developed three-dimensional Si network, and a highly-disordered low-dimensional SiH alloy region including voids [1]. In the former phase the hydrogen is randomly distributed, while in the latter, SiH clusters can develop. Morphology may be very sensitive to the preparation conditions, so that it is interesting to analyze the evolution of the microstructure as a function of the deposition temperature. We correlate the different morphological phases with the variation of the stretching modes at 2000-2100 cm^{-1} in the IR spectra, where the contribution at about 2000 cm^{-1} is related to the SiH mode, while that at 2070 cm^{-1} is associated to the presence of a defected, hydrogen rich, clustered phase (called SiH_c) that influences the transport properties. We have studied as physical parameters the minority carrier transport properties using the SSPG technique [2] in the ambipolar regime, and the majority ones with the photoconductivity. As already reported in literature [3], the complementarity of these two techniques gives the opportunity to study separately the $\mu\tau$ products for the two carriers as a function of the hydrogen content, defect density and Fermi level position. We report on the influence of the morphology induced defects on the transport properties of the two carriers, correlating the variation of the Fermi level position with the relative amount of the two morphological phases.

EXPERIMENTAL

Films were deposited on Corning 7059 glass and crystalline silicon substrates in a 13.56 MHz capacitively coupled PECVD multichamber system. A parallel electrode configuration (15 cm diameter) was used together with a grounded mesh electrode for the plasma confinement. The anode, heated by irradiation, was used as a substrate holder at a distance of about 2 cm from the cathode. The substrate temperature was controlled by using a thermoregulator and the temperature (T_d) measured with a thermocouple. Pure Silane was fed in the reactor and the flow rate kept constant at 50 sccm; the pressure was varied in the range 300-900 mTorr and

the net RF power in the range 2-10 Watt.

The optical analysis has been performed with standard methods, whereas the IR spectra have been collected with a PE 1760 FT-IR spectrophotometer. The total hydrogen content has been evaluated from the 640 cm^{-1} wagging mode, while the 2000-2070 cm^{-1} stretching peak has been resolved in its components by a standard fitting program. A 10 mW HeNe laser at 632.8 nm with a 500:1 polarization ratio was used for the SSPG while for the SSPC measurements a power density of 100 mW/cm^2 was fixed. In the SSPG an intensity ratio between the CW and the chopped beams of 20 was selected, and the drift field used for all the measurements was about 200 V/cm and low enough to satisfy the weak-field approssimation [4]. Within this approximation, the values determined by SSPG are ambipolar diffusion lengths (L_d).

The defect density (N_s) was evaluated from the subbandgap excess absorption obtained from the spectral photoconductivity measurement. The room temperature dark conductivity (σ_d) has been measured after annealing of the silver paste contacts at 10 °C below T_d for 30 min. The activation energy has been calculated from an Arrhenius plot, making the measurements in a cryostat in the 25-280 °C range.

RESULTS

Ambipolar diffusion lengths as a function of T_d for two different series of samples are reported in fig. 1, where two steps at about 165 and 220 nm are present. Moreover, in the inset L_d is drawn as a function of the pressure and RF power density for samples deposited at 213 and 260 °C, which correspond to the central position of the two steps.

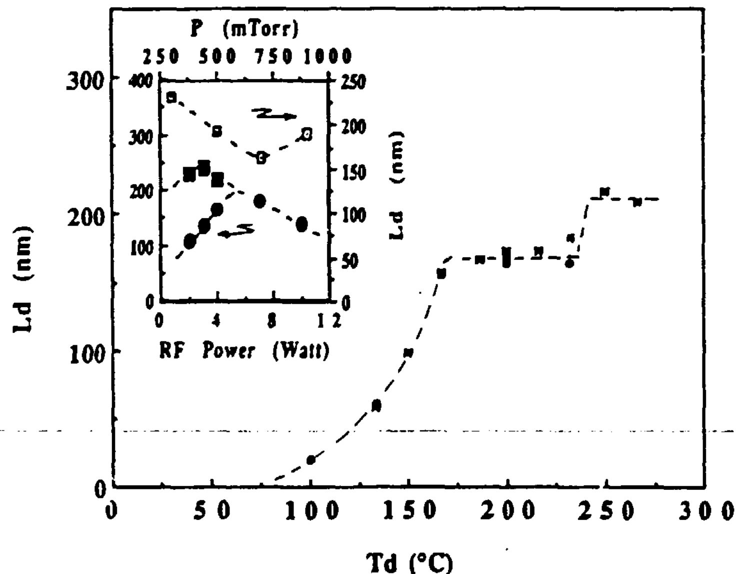

Fig. 1 - L_d vs T_d (4 W, 700 mTorr). Inset: L_d vs Pressure, 4 W, 213 °C (□); L_d vs RF Power, 700 mTorr, 213 °C (●) and 260 °C (■).

As we can see, keeping constant T_d and the RF power discharge, the dependence of L_d upon the pressure is weak and decreasing the pressure from 700 to 300 mTorr the L_d value rises up to 230 nm. The same effect can be obtained varying the RF power and the maximum value of L_d depends on T_d. As an overall behaviour, we can increase the L_d value either by decreasing the pressure and RF power or increasing the deposition temperature. This is in agreement with the commonly accepted criteria for obtaining electronic quality materials.

In fig. 2 we present the results of the IR analysis, as a function of the deposition temperature, for the total hydrogen and for the two contributions to the stretching mode. The oscillator strength and other optical constants needed for the hydrogen content calculations are taken from [5]. Whereas the total hydrogen content (H_{tot}) monotonically decreases with T_d approaching a plateau of about 8% around 220 °C, in the same temperature range the SiH_c decreases toward zero, and the SiH content varies from 10% to 7%.

In order to generalize our results and the following discussion, in the inset of fig. 2 we compare the bonded hydrogen percentage in our samples with results reported in literature [6]. The very good agreement allows us to derive conclusions on the hydrogen related material properties independently from the deposition apparatus.

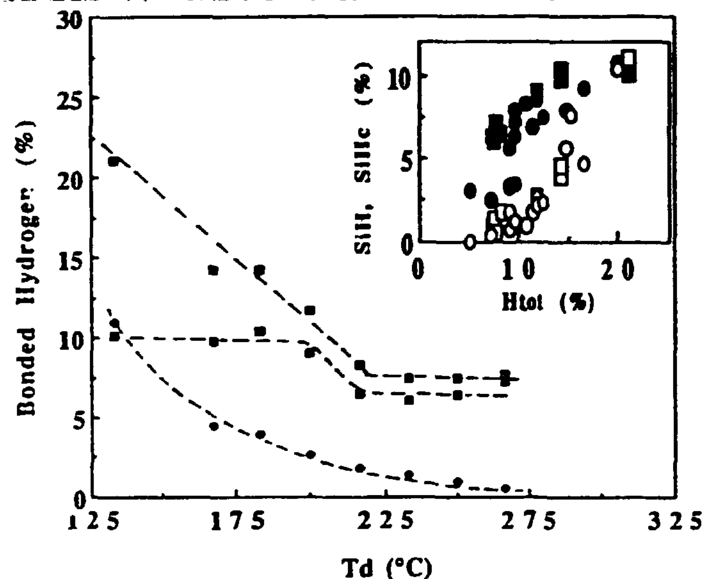

Fig. 2 - H_{tot} (□), SiH (■) and SiH_c (◆) vs T_d. Inset: this work (○), ref. [6].

From the plot of L_d against the hydrogen content we obtain the three curves reported in fig. 3.

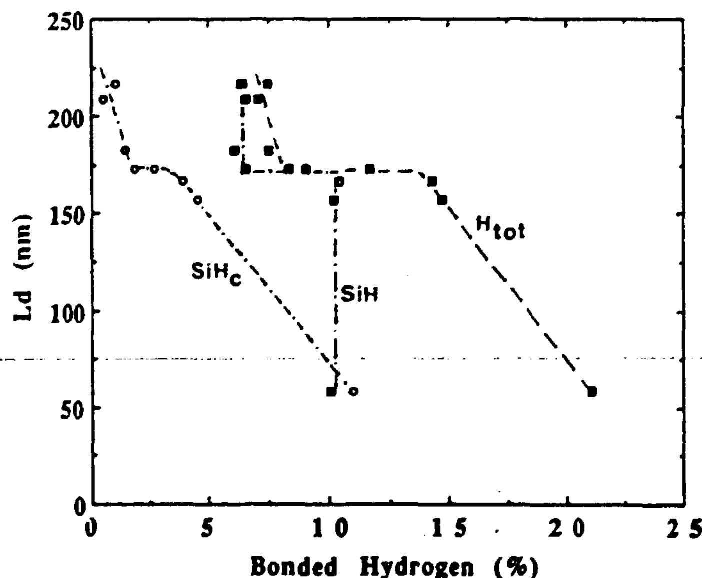

Fig. 3 - L_d vs Bonded Hydrogen (samples reported in fig. 1 (*)).

As can be seen, there are no big variations of L_d on SiH, so we can ascribe the overall dependence of L_d on hydrogen as only due to the SiH_c content. As a conclusion, we can affirm that to prepare electronic quality materials we must reduce the amount of clustered hydrogen below 1%, i.e. H_{tot} below 7%. We wish to remark that also in this representation of L_d we find a step around 165 nm. The same behaviour is once more obtained drawing L_d against the defects density N_s.

In order to correlate the photoelectronic properties of majority and minority carriers, in fig. 4 we report photoconductivity under AM1.5 (σ_{ph}) and dark conductivity (σ_d) as a function of L_d. As expected, an improvement of the minority carrier transport properties reflects also an increase of the majority carrier properties. The photosensitivity σ_{ph}/σ_d increases from 5 to $3*10^6$ when the L_d

changes from 20 to 240 nm.

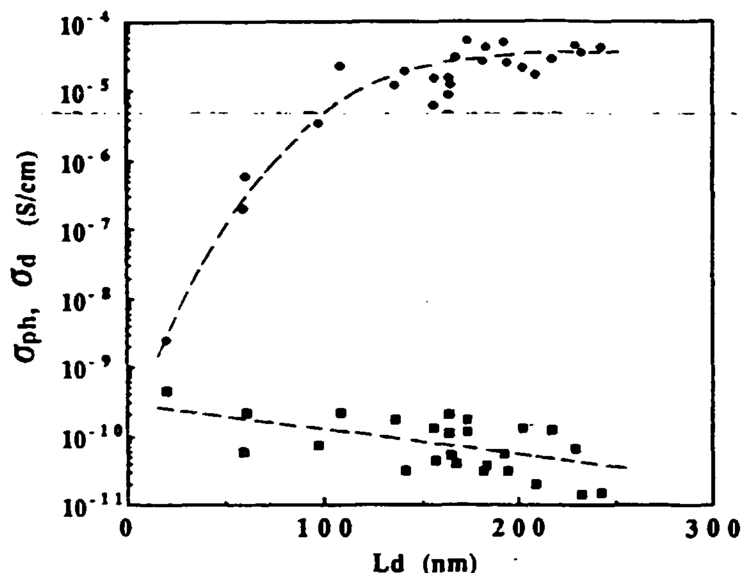

Fig. 4 - σ_{ph} (◆), σ_d (□) vs Ambipolar L_d.

Assuming that the transport takes place mainly in the extended states, we can extract both the electron and hole $\mu\tau$ products respectively from σ_{ph} and L_d measured at the same wavelength. In fig. 5 we report the obtained $\mu\tau$ values as a function of the measured N_S content: an intuitive explanation of this non-monotonic trend needs an in-depth analysis of the role played by the defect density on the transport. To this aim, we measured the dark Fermi level position respect to the valence mobility edge on the whole set of samples.

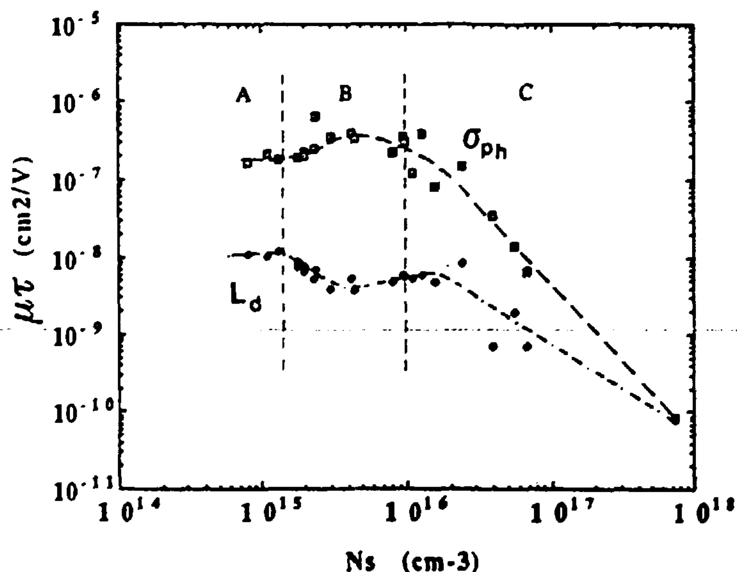

Fig. 5 - Majority (□) and minority (◆) carriers $\mu\tau$ product versus defect density (N_S).

In fig. 6 we show the values of the Fermi level energy (E_f') normalized to a unity value of the mobility gap, calculated by considering the mobility gap 10% higher than the measured optical gap, as a function of N_S. As we can see, defected materials exhibit an n-type behaviour, whereas, decreasing N_s below $3*10^{15}$ cm^{-3}, we observe a switch to p-type. We wish to remark that the involved variations of E_f' are well outside the experimental error. As a final step, in fig. 7 we report the minority and majority carriers $\mu\tau$ values as a function of E_f'. For the sake of clarity, in this picture we focus on the samples contained in regions A and B of fig. 6, assuming that the behaviour in region C may be simply explained as a general degradation of the electronic properties due to the high defect density ($N_s > 10^{16}$ cm^{-3}).

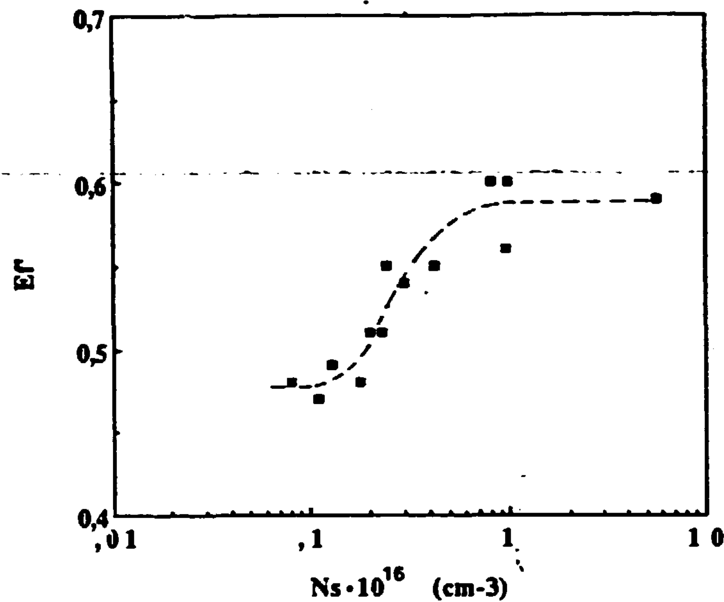

Fig. 6 - Normalized Fermi level energy (E_f') as a function of N_s.

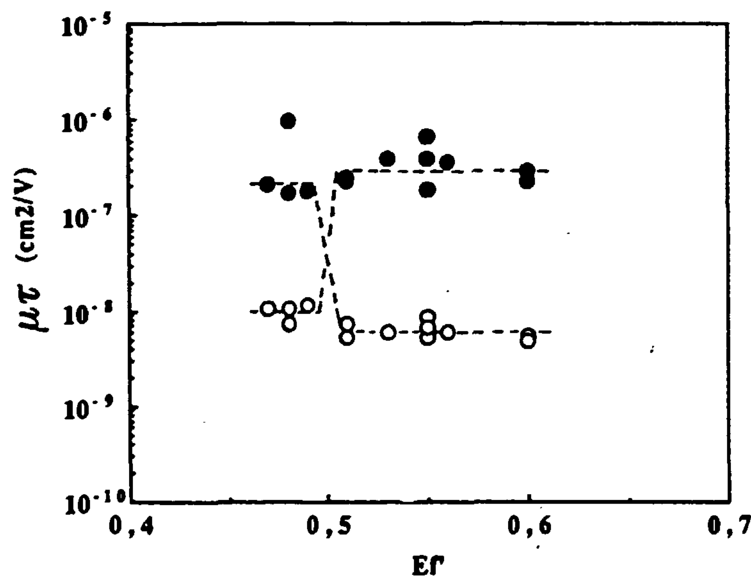

Fig. 7 - Majority (minority) carriers $\mu\tau$ value vs E_f'. Dotted lines indicate holes [●] (electrons [○]) below midgap and electrons [●] (holes [○]) upper midgap respectively.

DISCUSSION AND CONCLUSIONS

The discussion of experimental results stems from a morphology model where two different phases can be distinguished depending on the type of bonded hydrogen whose relative amount is forced by the variation of T_d. In this frame, good electronic materials, having high σ_{ph}/σ_d and high L_d, are characterized by a very low content of clustered hydrogen, obtained at T_d>250 °C, in spite of homogeneity and growth rate. We start the discussion from the E_f' dependence on N_s (fig. 6). High defect density materials are also SiH_c-rich and this implies a n-type behaviour of the semiconductor. This is well explained by a defect pool model which correlates the clustered-phase of the material to the presence of a large distribution of charged defects in the gap which pins E_f in a n-type position. When the SiH_c content lowers below 4%, the Fermi level lowers down in the gap, and the material switches to p-type, since the clustered hydrogen-induced defects have a negligible influence and E_f is now fixed by band tails and neutral dangling bonds. The model and simulation results is going to be discussed.

As we said, the behaviour of the Fermi level, as well as that of majority and minority carrier transport properties can be explained by a simple model of density

of electronic defects. This model is based on the assumption of two distinct species of localized states in the gap: a) hydrogen induced positively and negatively charged traps, described by two wide Gaussian distributions, positioned respectively above and below the Fermi level; b) neutral defects positioned just below midgap. The exact position of E_f around midgap is determined by the relative weights of charged and neutral defect distributions.

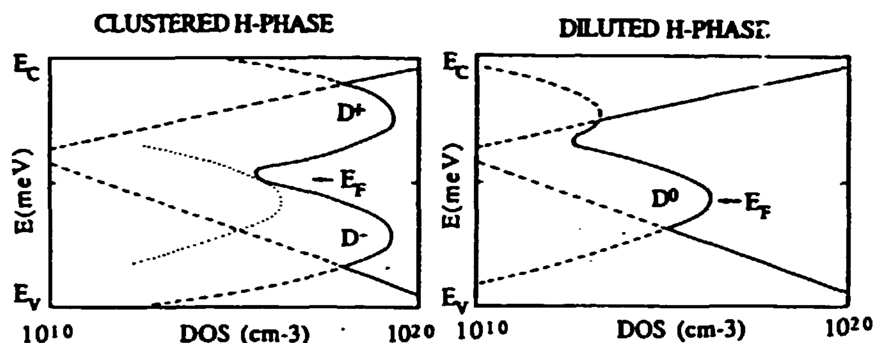

Fig. 8 - Defect-pool maded results. Fermi level position as a function of relative amount of clustered and diluted hydrogen phase. D^o, D^+, D^- indicates neutral, empty, occupied defective states.

For example, referring to fig. 8 we see that E_f is pinned at the deep minimum between the two large distributions of charged defects, being negligible the contribution from the low density of neutral defects, (in this case we have a n-type behaviour); on the contrary, when the relative weight of neutral to charged defects increases, E_f shifts toward the valence bandtail and we have a p-type behaviour.

This E_f switch from n-type (in the clustered rich-phase) to p-type (in the diluted hydrogen phase) material gives rise to the plateau in the L_d versus hydrogen content curves (fig. 3). On the basis of these argumentations, we can explain the $\mu\tau$ values deduced from σ_{ph} as due to majority carriers being holes or electrons, depending on the amount of SiH_c, and the $\mu\tau$ deduced from L_d as due to minority carriers, respectively in the diluted hydrogen and in the clustered phases. The complementary nature of the employed techniques allows us to monitor this carrier inversion. The concept of the inversion of majority (minority) carrier in undoped a-Si:H affecting the $\mu\tau$ product has been previously suggested by Abel and coworkers [3], modelling the SSPG and SSPC techniques, and supports the experimental results on compensated materials by Yang and coworkers [7]. In conclusion, on the basis of experimental results obtained from structural and electronic measurements performed on a wide set of samples, we propose a morphology model of a-Si:H based on the existence of a two hydrogen-ruled phases of the material. The relative amount of the two co-existing phases determines the density of states in the gap, fixes the Fermi level position and the majority and minority carrier transport. In particular, a high density of charged traps is correlated to clustered-hydrogen rich material and gives rise to a n-type behaviour; predominant neutral defects are attributed to a hydrogen-diluted phase and gives rise to a p-type behaviour.

REFERENCES

1. - A.A. Langford, M.L. Fleet, B.P. Nelson, W.A. Lanford, N. Maley; Phys. Rev. B45, 13367 (1992)
2. - D. Ritter, E. Zeldov, K. Waiser; Appl. Phys. Lett. 49, 791 (1986)
3. - C.D.Abel, G.H. Bauer MRS Symp. 1992, San Francisco (CA)
4. - K. Hattori, H. Okamoto, Y. Hamakawa; Phys. Rev. B45, 1126 (1992)
5. - H. Shanks, C.J. Fang, L. Ley, M. Cardona, F.J. Demond, S. Kalbitzer; Phys. Stat. Sol. 100, 43 (1980)
6. - J. Shirafuji, M. Kuwagaki, S. Nagata; J. non-Cryst. Solids 72, 199 (1985)
7. - L. Yang, A. Catalano, R.R. Arya, I. Balberg; Appl. Phys. Lett. 57, 908 (1990)

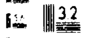

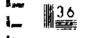

MICROCOPY RESOLUTION TEST CHART
NATIONAL BUREAU OF STANDARDS
STANDARD REFERENCE MATERIAL 1010a
(ANSI and ISO TEST CHART No. 2)